PROCEEDINGS OF THE ROYAL SOCIETY A

rspa.royalsocietypublishing.org

Research

Article submitted to journal

Subject Areas:
Southern Ocean processes, remote sensing, physical oceanography

Keywords:
Antarctic Circumpolar Current, Southern Annular Mode, climate change, wind forcing

Author for correspondence:
Sarah Gille
e-mail: sgille@ucsd.edu

Meridional Displacement of the Antarctic Circumpolar Current

Sarah T. Gille

Scripps Institution of Oceanography, University of California San Diego, 9500 Gilman Dr., Mail Code 0230, La Jolla, CA 92093-0230, USA

Observed long-term warming trends in the Southern Ocean have been interpreted as a sign of increased poleward eddy heat transport or of a poleward displacement of the entire Antarctic Circumpolar Current (ACC) frontal system. The two-decade-long record from satellite altimetry is an important source of information for evaluating the mechanisms governing these trends. While several recent studies have used sea surface height contours to index ACC frontal displacements, here altimeter data are instead used to track the latitude of mean ACC transport. Altimetric height contours indicate a poleward trend, regardless of whether they are associated with ACC fronts. The zonally-averaged transport latitude index shows no long-term trend, implying that ACC meridional shifts determined from sea surface height might be associated with large-scale changes in sea surface height more than with localized shifts in frontal positions. The transport latitude index is weakly sensitive to the Southern Annular Mode (SAM) but is uncorrelated with El Niño Southern Oscillation (ENSO).

1. Introduction

The Southern Ocean, the winds that force it, and the cryosphere to its south have experienced distinct patterns of change over the past five to six decades. In the ocean, evidence from historic hydrographic data and newer temperature profiles indicates rising temperatures over a broad range of depths extending well below the ocean surface [1–5]. Southern Ocean warming is concentrated in the circumpolar band corresponding to the Antarctic Circumpolar Current (ACC). In the top 1000 m of the ocean approximately 80% of the net heat content increase in the Southern Hemisphere oceans appears to have occurred south of 30°S, largely within the ACC [2]. A

number of studies have noted that the warming trend identified in the ACC region has been characterized as being consistent with displacing the ACC poleward by about 1° latitude every 35 years [2,6,7], although poleward displacement of the current would not be expected to be uniform, since the ACC is topographically constrained in some locations and more free to migrate in other areas [8,9].

In the cryosphere, the most rapid melting of glaciers on the Antarctic continent has occurred in West Antarctica, particular for glaciers with outlets in the Amundsen Sea Embayment, though also near 80°E and 120°E [10]. Regions of rapid glacial melting share a common trait: they are all at locations where the ACC flows near the Antarctic continent. This has led to speculation that changes in the ACC could be responsible for delivering supplemental warm Circumpolar Deep Water to the Antarctic marginal seas, thus contributing to basal melting of the Antarctic ice shelves, and reducing the efficacy of the ice shelves in buttressing the continental glaciers [11,12].

Finally, winds that drive the ACC, as indexed by the Southern Annular Mode (SAM), have increased over the past several decades [13,14]. The SAM is a measure of the pressure difference between Antarctic and mid-latitudes, and increases in the SAM translate into winds that are both stronger and further poleward. Modeling studies indicate that both ozone depletion and greenhouse warming can strengthen the SAM [15–18], thus implying that SAM trends may change in the future, as ozone begins to recover while greenhouse forcing continues.

Taken together, these observations suggest a hypothesis that the long-term strengthening of the SAM has resulted in a poleward shift in the ACC, which in turn has perhaps brought more warm Circumpolar Deep Water south to the periphery of the Antarctic continent. One of the goals of this paper is to explore whether this hypothesis is consistent with available observations.

The SAM is not the only mode of variability at work in the Southern Ocean [19]. In particular, El Niño/Southern Oscillation (ENSO)-related temperature variability in the central tropical Pacific correlates with sea-ice extent and sea surface temperature (SST) [20], wth mixed-layer depth in the Pacific sector of the Southern Ocean [21], with warming in West Antarctica [22], and with upper-ocean heat content in Drake Passage [23].

This study specifically focuses on the ACC component of Southern Ocean climate processes. Other recent studies have explored the ocean-cryosphere links in greater detail by asking how heat traverses the ACC to influence ocean heat content in Antarctic marginal seas in a way that might influence glacial stability [24–27]. Heat transport from mid-latitudes into the Southern Ocean is also potentially important as an oceanic source of heat and has been explored elsewhere: in one recent assessment of Argo float data, poleward heat transport across 32°S in the Pacific Ocean appears more closely linked to the SAM than to ENSO [28].

The goal of this study is to focus specifically on the temporal variability of the position of the Antarctic Circumpolar Current and its links to the SAM and ENSO. Section 2 reviews recent work to assess variability in the ACC, Section 3 explains the data and methods used for this analysis, Section 4 describes the results, and Section 5 summarizes the findings.

2. Frontal Displacement in the Southern Ocean

Projections from climate models have provided a clear picture of how the ACC as a whole might be expected to respond to a changing climate. In the atmosphere, most projections indicate that a warming climate should be accompanied by a poleward displacement in the winds [29] and correspondingly a poleward displacement of the ACC [15,30–33]. However, these trends are not clear in satellite-era reanalysis wind fields [33], and 20th century trends emerge largely as summer effects associated with ozone depletion [18].

From observations, the ACC is characterized as consisting of multiple narrow frontal jets. From north to south, these are traditionally termed the Subantarctic Front, the Polar Front, and the Southern ACC Front [34]. Fronts typically represent sharp density or temperature gradients and can mediate air-sea heat exchange, with significant gradients at the fronts [35,36]. However the focus of this study is on transport and meridional migration of fronts rather than their role in heat

fluxes. The Rossby radius in the Southern Ocean is comparatively small [37], which means that the fronts can be less than 100 km wide. Thus efforts to understand meridional shifts in the ACC have typically focused on identifying meridional shifts in each of the fronts. Historical hydrographic data are sparse and inadequate for exploring how the ACC fronts have migrated over time, except in Drake Passage [6] and south of Tasmania [7], where repeat surveys have been carried out with eXpendable Bathythermographs (XBTs). Paleo-climate data generally suggest that ACC fronts were further north during the Last Glacial Maximum, but evidence does not appear sufficient to evaluate whether this was linked to a change in winds or whether other mechanisms contributed to this [38]. Most climate models are run at relatively coarse spatial resolution and do not represent mesoscale eddies. The models therefore cannot capture the detailed frontal structure of the ACC or its response to wind (which can include generation of mesoscale eddies).

From satellite data, some efforts have been carried out to study frontal migration from SST data [9,39,40], but infrared SSTs are blocked by clouds [39,40], and microwave SST observations have only been available since 2002, so do not provide a record sufficient to examine decadal-scale changes in the ACC fronts. Nonetheless, a 3-year analysis of Polar Frontal position from microwave SST provides evidence that changes in the mean latitude of the winds over the Southern Ocean lead changes in the mean latitude of the Polar Front [9].

The most extensive modern data set that can be used to assess changes in the position of the ACC comes from satellite altimeters, which have provided consistent time series of sea surface height (SSH) since the launches of ERS-1 in 1991 and TOPEX-Poseidon in 1992. Altimetric SSH data are useful for studying ocean variability, but are more challenging for inferring time-mean ocean circulation, because the Earth's geoid accounts for the vast majority of the time-mean SSH measured by the altimeter. The oceanographically relevant component of the mean sea surface, the mean dynamic topography (MDT), represents approximately 1% of the spatial variability in the mean SSH. While there are strategies available for inferring the positions of large-scale currents from the temporal variability alone [8,41–43], these approaches are not easily adapted to account for multiple fronts. Thus most recent studies have used an independent estimate of the MDT [44–47] in order to evaluate the time-varying and time-mean components of geostrophic velocities. MDT fields should be approached with caution: in the Southern Ocean MDT fields differ substantially, the MDT fields have been developed without oceanographic transport constraints, and they typically imply inconsistent transport changes between the "choke points" of the ACC, at Drake Passage, south of Africa, and south of Australia [48].

Nonetheless, by using an estimate of the MDT in conjunction with altimetric variability, oceanographic investigations have been able to characterize eddy-meanflow interactions [49] and also the time-varying structure of the ACC fronts [21,50–52]. The time-varying dynamic ocean topography at latitude θ and longitude ϕ is:

$$h(t,\theta,\phi) = \mathrm{MDT}(\theta,\phi) + h'(t,\theta,\phi), \tag{2.1}$$

where h' is the SSH anomaly from altimetry and MDT is the mean dynamic topography, estimated by differencing the geoid and mean SSH. Zonal surface velocity is related to meridional gradients in h through the geostrophic relationship:

$$u_g = -\frac{g}{f}\frac{2\pi}{L}\frac{\partial h(t,\theta,\phi)}{\partial \theta}, \tag{2.2}$$

where g is gravity, f is the Coriolis parameter and is negative in the Southern Hemisphere, θ is assumed to be in radians, and L is the circumference of the Earth.

Fronts in the Southern Ocean are expected to coincide with strong gradients in h and correspondingly with strong geostrophic velocities. A recent analysis of altimetric gradient variability concluded that each of the three major ACC fronts has multiple branches each associated with an elevated gradient in h [50,51]. Over time the fronts meander and vary in strength, but they nonetheless have been assumed to be associated with fixed contours of h. This approach implies that all of the branches of the ACC fronts appear to have trended southward

during the first 15 years of the altimeter record, implying about a 60 km southward shift in 15 years, consistent with a long-term southward displacement of the fronts [52].

Analysis of SSH displacements on regional scales implies more nuanced variability. On time scales less than 3 months, the SAM dominates and is positively correlated in the Pacific and anti-correlated in the Indian Ocean [21]. In contrast, on time scales greater than a year, the fronts tend to be anti-correlated with the Niño 3.4 ENSO index [21]. These patterns differ from the southward annular displacement of the ACC suggested by multi-decadal analyses [1,2].

The altimeter-based analyses of ACC frontal variability [21,50–52] leave a number of open questions. First, as noted by [52], long-term trends in the position of SSH contours could be explained either by dynamically driven frontal displacements or by large-scale increases in sea level, possibly associated with steric height changes due to warming of the ocean. When fixed height contours are used to identify frontal positions, there is not an easy way to separate these effects. As [53] showed from eddy-resolving model output, jets can be intermittent, and when jets dissipate, the SSH contours identified to the jets can migrate substantially. Second, tracking temporal variations in the ACC by tracking each of the fronts is a daunting task, given that the ACC appears to consist of eight quasi-stationary fronts [51], that vary in a spatially inhomogeneous way in response to remote forcing in different ocean basins [21]. For example, we might hypothesize that the ACC could respond to changing winds over the Polar Front either by having each of the individual branches of the Polar Front meander or alternatively by having the strength of the southern branch of the Polar Front change relative to the strength of the northern branch of the Polar Front, with minimal meandering of either front. This suggests that if our real goal is to know the latitude of the water that is advected eastward as part of the ACC, then detailed tracking of the individual branches of the ACC fronts is not important, and instead we simply need a robust method to determine the mean latitude of the eastward transport. (The situation would be different if our primary goal were to identify the latitude of sharp temperature gradients that locally influence air-sea fluxes.)

This study focuses on assessing changes in the latitude of mean ACC transport, in order to minimize the sensitivity of the results to the details of the jet position and strength or dynamic ocean topography labels. The mean latitude of the eastward surface transport is computed as:

$$\overline{\theta(t,\phi)} = \frac{\int_{\theta_S}^{\theta_N} \theta u_g d\theta}{\int_{\theta_S}^{\theta_N} u_g d\theta}. \tag{2.3}$$

In essence, $\overline{\theta}$ represents the transport weighted average latitude, and it is computed by using surface geostrophic velocity u_g as a weight. Thus if the northern and southern integration limits (θ_N and θ_S) are in relatively low velocity regions, (2.3) provides a simple measure of meridional variation in ACC transport that will be independent of large-scale steric warming and cooling of the Southern Ocean.

3. Data and Methods

Like previous altimeter-based studies of frontal variability [21,50–52], this study takes advantage of gridded SSH anomaly data distributed by Aviso [54,55]. Sea surface height anomalies are released on a $1/3^\circ$ by $1/3^\circ$ Mercator grid at weekly time intervals, and in this analysis they span the time period extending from 14 October 1992, just after the launch of the TOPEX/Poseidon altimeter, through 26 December 2012. This study uses the "reference" gridded data, which nominally combine data from one satellite on the ERS/Envisat orbit and one satellite from the TOPEX/Poseidon/Jason orbit. With this sampling pattern, the Aviso product achieves an effective spatial resolution of about 3° and effective temporal resolution of 20 days [56].

For this study, the time-varying dynamic ocean topography h is computed by adding an MDT to the SSH anomalies from Aviso. The time-varying dynamic ocean topography can be sensitive to the choice of MDT [48], so for this study two products are tested. One is based on the difference between the Danish National Space Center 2008 (DNSC08B) mean sea surface from altimetry

and the Earth Gravitational Model 2008 (EGM08) geoid, which is computed from gravity data only [46]. The second is released by Aviso and is based on gravity data and altimetry, augmented with in situ oceanographic data to provide more high resolution structure to the dynamic ocean topography [44,45]. For most aspects of the analysis, distinctions between MDTs prove not to be significant, and here plotted results will be based on the Aviso MDT.

The variability of the ACC position is compared against proxies for large-scale climate patterns based on the SAM and ENSO indices distributed by the Ocean Observations Panel for Climate (OOPC) and the Joint World Meteorological Organization–International Oceanographic Commission Technical Commission for Oceanography and Marine Meteorology (JCOMM) Observations Programme. As a measure of ENSO variability, this study uses the Niño 3.4 index, computed from the optimum interpolation SST analysis [57] in the central tropical Pacific. As a measure of the SAM, the National Weather Service Climate Prediction Center's Antarctic Oscillation index is used. This is computed from the leading empirical orthogonal function of 700-hPa height anomalies, as determined in NCEP/NCAR reanalysis data [58].

4. Results

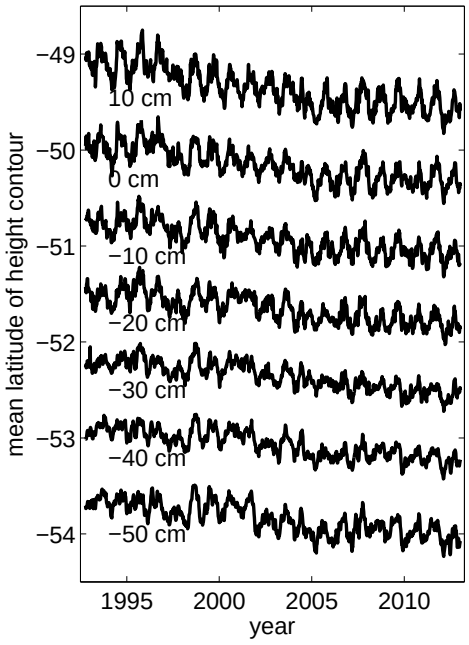

Figure 1. Time series of latitudes of SSH contours, computed using the Aviso mean dynamic topography [44,45] and SSH anomalies. Circumpolar SSH contours are identified by height, and are defined following [45] so that the zero height contour is roughly in the Subantarctic Front.

Previous studies have typically used the latitudinal positions of fixed SSH contours h as a measure of ACC frontal variability [21,50–52] to be compared with SAM or ENSO-related climate fluctuations. Thus as a starting point, Figure 1 shows time series of SSH contour latitudes. A range of SSH contours are plotted, but they have not been identified with specific fronts: some of them are likely associated with strong SSH gradients, but others may be in regions of weaker flow. In Figure 1, all of the SSH contours shift in latitude in parallel, implying that the latitudinal shifts are not sensitive to whether SSH contours are in fronts or between fronts. The largest effects for all SSH contours are associated with the annual cycle in steric expansion of the ocean: a sinusoidal

annual cycle explains between 27% and 52% of the variance, depending on the height contour (with minor differences for the two different mean dynamic ocean topography choices). Even once the annual signal has been removed from the time series of SSH contour latitudes, the latitudinal variations in SSH contours have correlation coefficients that exceed 80%. This suggests that SSH contour displacement depends on meridionally consistent changes in SSH rather than on detailed displacements of individual fronts.

The latitudinal shifts in SSH contours vary depending on longitude, but the long-term trend over the duration of the altimeter record generally indicates a poleward shift in SSH contours, except in the central Pacific, as illustrated in Figure 2a. This is consistent with patterns of regional sea level rise [59]. For the latitude range from 40 to 60°S, altimeter data indicate that a 60 km southward shift in sea surface height contours is also consistent with a mean increase in sea level of 2.9±0.1 mm yr^{-1} (where here the uncertainty is the standard error, computed as the standard deviation of all pixels divided by the square root of the number of degrees of freedom, here taken to be 1800.) This trend agrees with the observed global trend of 3.2±0.4 mm yr^{-1} [59], suggesting that the trend at the locations of the ACC fronts is typical of the global ocean. Thus rather than indicating meridional displacement of strong fronts, the long-term trends in latitude of SSH contours could be a sign of wide-spread sea-level rise (e.g. through steric expansion of the ocean through upper ocean heating, which can raise h without necessarily reposition the geostrophic jets defined by peaks in u_g.)

The latitude of mean transport defined by (2.3) is intended to be less sensitive than SSH contour position to steric expansion. Figure 2b shows the time mean latitude of ACC transport, based on $\overline{\theta}$, here integrated between the mean latitudes of the -60 cm and +30 cm mean dynamic topography contours from [45]. Also shown in Figure 2b with solid lines are the one-standard deviation northern and southern ranges of the time varying values of $\overline{\theta}$. The central latitude varies slowly with longitude, with the exception of one spike around 300°E, at Drake Passage. Flow is furthest north in the Atlantic, and furthest south in the eastern Pacific.

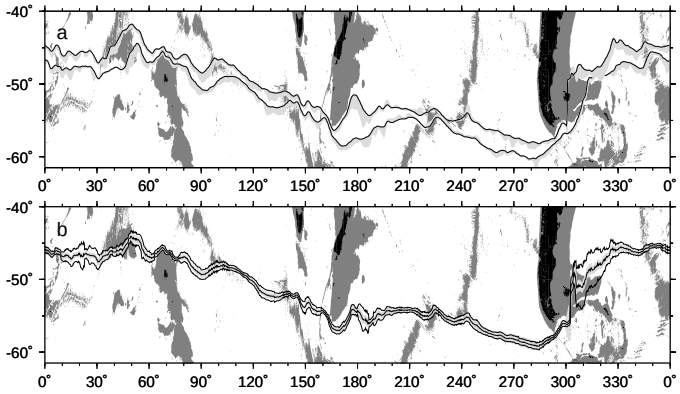

Figure 2. (a) (Solid lines) Mean position of -30 cm and 0 cm contours (see Figure 1) as a function of longitude. Linear trends fitted to the 20-year altimeter record are plotted as light-gray regions, here indicating the net displacement over 20 years. (Note that trends are plotted relative to the time mean position, so this does not represent the extreme latitudes achieved after 20 years.) Other contours show similar trends. (b) (Solid lines) Mean central latitude of ACC transport as computed from the time average of $\overline{\theta(t,\phi)}$ and one standard deviation ranges, computed from the temporal variability. Here results are based on the mean dynamic topography from Aviso [44,45]. Light shaded gray indicates the one-standard deviation range of $\overline{\theta(t,\phi)}$, as obtained using a Monte Carlo simulation with variable end latitudes, as discussed in the text. In both panels, dark shaded gray areas indicate regions with bathymetry shallower than 3000 m. The map projection is exagerated in the meridional direction in order to highlight the latitude ranges.

The results are sensitive to choice of integration limits θ_S and θ_N. To evaluate this, 100 realizations of a Monte Carlo simulation were performed, in which θ_S and θ_N were both randomly perturbed using Gaussian random numbers with a standard deviation of 5° latitude. The light gray shading round the mean $\overline{\theta}$ in Figure 2 indicates the ± 1 standard deviation range of mean $\overline{\theta}$ from the 100 Monte Carlo realizations. In general the gray region is narrower than the 1-σ range in solid lines that is determined from temporal variability.

Figure 3 shows a Hovmöller diagram of temporal anomalies of the mean latitude of ACC transport, $\overline{\theta(t,\phi)}'$. The results in Figure 3 show highly variable spatial and temporal variability, without obvious long-term trends, in contrast with the equivalent plot computed based on the latitude of a fixed SSH contour (not shown). Anomalies show some evidence of eastward or westward propagation over distances of a few 100 km, but do not appear to propagate across entire ocean basins.

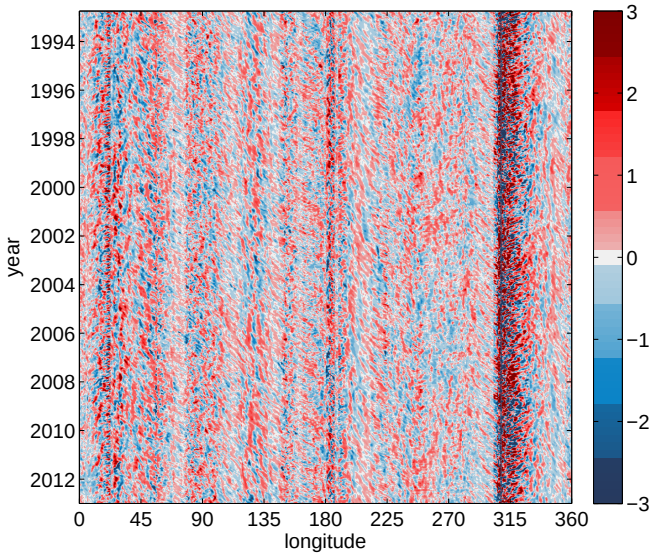

Figure 3. Hovmöller diagram showing the temporal and longitudinal structure of anomalies in the latitude of mean ACC transport $\overline{\theta(t,\phi)}$. Anomalies are measured in degrees latitude. Here, the mean dynamic topography from Aviso is used [44,45]; results are similar with the EGM08/DNSC08B mean dynamic topography [46].

The time series in Figure 3 were cleaned by removing anomalous meridional shifts exceeding 8° latitude. In these tests, for 20 years of data at monthly temporal resolution, correlations should exceed 0.126 to be judged statistically significant at the 95% level. As a function of longitude, $\overline{\theta(t,\phi)}'$ is significantly correlated with the Niño 3.4 index at 22% of longitudes tested and with the SAM index at just 11% of longitudes (not shown.) This implies the possibility of a regional correlation between the Niño 3.4 index and transport variability. However, correlations are not particularly strong, and they vary substantially with longitude, with both positive and negative correlation coefficients observed. Similarly, results based on SSH contour shifts, have also implied significant regional differences in correlations with the SAM or Niño 3.4 indices [21].

The zonal average of Figure 3, $\langle\overline{\theta(t)}'\rangle$, is shown in blue in the upper panel of Figure 4, normalized by the standard deviation, which is 0.049° latitude. (Here angular brackets indicate zonal or along-stream averages.) This provides a measure of the large-scale response of the ACC transport to the extent that it is zonally coherent. This index of ACC variability shows no long-term trends, in striking contrast with the long-term trends in SSH contours [52] shown in Figure 1. The lack of trend is insensitive to random variations in the northern and southern

limits of integration by up to ±20 cm. This suggests that in the aggregate, the ACC transport has not shifted meridionally during the 20-year altimeter record. Similarly, in an eddy-resolving model, [53] found that long-term changes in the wind resulted in no long-term displacement of the ACC.

Also shown in the upper panel of Figure 4 are time series of the SAM (green) and Niño 3.4 (red) indices, here computed by interpolating monthly climate indices onto the dates of the weekly Aviso altimetry. On monthly time scales there is no evidence of statistically significant correlation between the ACC position variability in Figure 4 and either climate index.

In the lower panel of Figure 4 the $\langle \overline{\theta(t)}' \rangle$ and SAM time series have been filtered using a two-year wide triangle filter. This smoothing removes high-frequency fluctuations leaving only interannual signals, and in this case the SAM is weakly anti-correlated with $\langle \overline{\theta(t)}' \rangle$, at roughly the 90% significance level. These results are sensitive to the choice of mean dynamic topography. More anomalous spikes in transport latitude appear when EGM08/DNSC08B mean dynamic topography is used, and in that case the signals are anti-correlated at only about the 65% significance level. In neither case is a significant correlation found between the Niño 3.4 index and $\langle \overline{\theta(t)}' \rangle$.

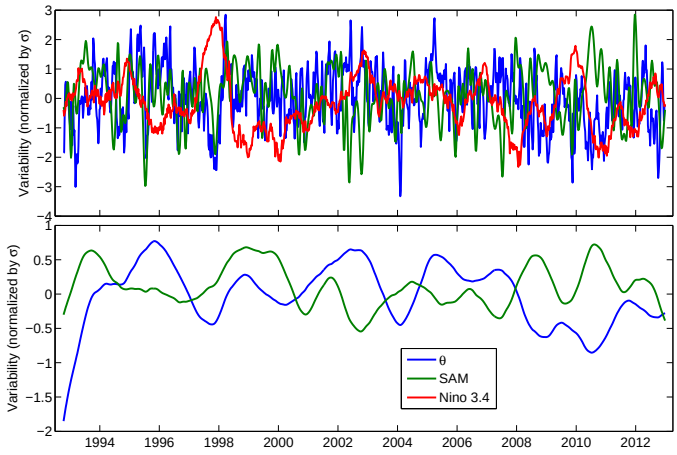

Figure 4. (top) Unfiltered time series of the along-stream average mean latitude anomaly of ACC transport, $\langle \overline{\theta(t)}' \rangle$ (blue line), and the SAM (green) and Niño 3.4 (red) indices. (bottom) Time series of $\langle \overline{\theta(t)}' \rangle$ (blue) and SAM (green) smoothed with a two-year wide triangle filter. For $\langle \overline{\theta(t)}' \rangle$, the mean dynamic topography from Aviso is used [44,45].

The results of this analysis suggest that latitudinal shifts in the circumpolarly-integrated ACC transport are more correlated with the SAM than with the Niño 3.4 index, implying that zonally-averaged Southern Hemisphere winds have more impact on the mean latitude of the ACC than do remote tropical teleconnections. The low correlation with Niño 3.4 is not surprising since ENSO impacts are not expected to be zonally coherent. The findings should be interpreted with caution, since even on interannual scales, the correlation between the SAM and $\langle \overline{\theta(t)}' \rangle$ does not pass a rigorous 95% statistical significance test. Coherence analysis or lagged correlations would make it possible to assess time lags in the relationships between $\langle \overline{\theta}' \rangle$ and climate indices, but that is beyond the scope of this short paper.

5. Summary and Conclusions

This study has used altimeter data to examine temporal shifts in the position of the ACC. In contrast with earlier altimeter-based studies [21,50–52], this analysis has not focused on latitudinal shifts in SSH contours, which are potentially sensitive to large-scale steric expansion

associated with warming of the Southern Ocean, and which therefore do not provide clear insights into driving mechanisms. Instead, this study has explored an alternate measure of ACC displacement, in this case based on the latitude of the mean, meridionally-averaged transport, $\overline{\theta(t,\phi)}$. This transport latitude index is designed to minimize large-scale steric height signals, though it is sensitive to the definition of end points and to some extent to the MDT.

On the basis of the position index, $\langle\overline{\theta}\rangle$, the zonally-averaged latitude of ACC transport shows no long-term, in contrast the SSH-contour based measures of ACC variability. This leaves open the questions of what mechanisms account for the long term warming observed in the Southern Ocean in recent decades and whether more warm Circumpolar Deep Water is reaching the Antarctic ice edge. Analyses of hydrographic data suggest that the Southern Ocean warming signal is too deep to be explained trivially through air-sea fluxes [2]. While it remains possible that the ACC fronts have shifted poleward in a way that has not yet been convincingly diagnosed, an alternative is that enhanced meridional heat transport, perhaps via eddy heat fluxes, may account for the observed warming. Further analysis of the ocean heat budget will be needed to unravel these mechanisms.

The zonally-averaged position index $\langle\overline{\theta(t)}\rangle$ is uncorrelated with the Niño 3.4 index on any timescales. In contrast, $\overline{\theta(t,\phi)}$ does correlate with the Niño 3.4 index, with differing correlations as a function of longitude. The nature of the Niño 3.4 correlation suggests that tropical Pacific influences on the Southern Ocean are regional and not circumpolarly coherent. The circumpolarly-averaged value $\langle\overline{\theta(t)}\rangle$ is weakly anti-correlated with the SAM index, implying that changes in the latitude and strength of the wind that are represented by the increasing SAM, might be able to displace the mean transport of the ACC poleward. Taken together, these results are suggestive of a two-mechanism system, in which regional effects associated with upper ocean temperatures, air-sea fluxes, and even ice melt may respond to changes in the tropical Pacific [21–23], but the latitude at which the zonally-averaged ACC carries its mean transport might be more dependent on the SAM-related winds than on teleconnections with the equatorial Pacific.

Acknowledgment

The altimeter products were produced by Ssalto/Duacs and distributed by Aviso with support from CNES. The DNSC08B-EGM08 dynamic ocean topography is made available by the National Geospatial-Intelligence Agency (http://earth-info.nga.mil/GandG/wgs84/gravitymod/egm2008/oceano.html). Ocean climate indices for SAM and ENSO for this study were distributed by the Ocean Observations Panel for Climate (OOPC) and the JCOMM Observations Programme (http://stateoftheocean.osmc.noaa.gov/). The work discussed here has benefited from discussions with Angelica Gilroy, Doug Martinson, Matt Mazloff, Rosemary Morrow, Dean Roemmich, Uriel Zajaczkovski, and Nathalie Zilberman. Many thanks also to the anonymous reviewers for their insightful suggestions. Work has been supported by a number of funding sources, including NOAA award NA10OAR4310139, NSF grant OCE-1234473, and NASA grant NNX13AE44G.

References

1. Gille, S. T., 2002 Warming of the Southern Ocean since the 1950s. *Science* **295**, 1275–1277.
2. Gille, S. T., 2008 Decadal-scale temperature trends in the Southern Hemisphere ocean. *J. Climate* **21**, 4749–4765.
3. Böning, C., Dispert, A., Visbeck, M., Rintoul, S. R. & Schwarzkopf, F. U., 2008 The response of the Antarctic Circumpolar Current to recent climate change. *Nature Geosci.* **1**, 864–869.
4. Purkey, S. G. & Johnson, G. C., 2010 Warming of global abyssal and deep Southern Ocean waters between the 1990s and 2000s: Contributions to global heat and sea level rise budgets. *J. Climate* **23**, 6336–6351.

5. Purkey, S. G. & Johnson, G. C., 2013 Antarctic Bottom Water warming and freshening: Contributions to sea level rise, ocean freshwater budgets, and global heat gain. *J. Climate* **26**, 6105–6122.
6. Sprintall, J., 2008 Long term trends and interannual variability of temperature in Drake Passage. *Prog. in Oceanogr.* **77**, 316–330.
7. Morrow, R., Valladeau, G. & Sallée, J. B., 2008 Observed subsurface signature of Southern Ocean sea level rise. *Prog. Oceanogr.* **77**, 351–366.
8. Gille, S. T., 1994 Mean sea surface height of the Antarctic Circumpolar Current from Geosat data: Method and application. *J. Geophys. Res.* **99**, 18,255–18,273.
9. Dong, S., Sprintall, J. & Gille, S. T., 2006 Location of the Polar Front from AMSR-E satellite sea surface temperature measurements. *J. Phys. Oceanogr.* **36**, 2075–2089.
10. Rignot, E., Bamber, J. L., van den Broeke, M. R., Davis, C., Li, Y., van de Berg, W. J. & van Meijgaard, E., 2008 Recent Antarctic ice mass loss from radar interferometry and regional climate modelling. *Nature Geosci.* **1**, 106–110.
11. Jacobs, S. S., Jenkins, A., Giulivi, G. F. & Dutrieux, P., 2011 Stronger ocean circulation and increased melting under Pine Island Glacier ice shelf. *Nature Geosci.* **4**, 519–523.
12. Pritchard, H. D., Ligtenberg, S. R. M., Fricker, H. A., Vaughan, D. G., van den Broeke, M. R. & Padman, L., 2012 Antarctic ice-sheet loss driven by basal melting of ice shelves. *Nature* **484**, 502–505.
13. Thompson, D. W. J., Wallace, J. M. & Hegerl, G. C., 2000 Annular modes in the extratropical circulation. Part II: Trends. *J. Climate* **13**, 1018–1036.
14. Marshall, G. J., 2003 Trends in the Southern Annular Mode from observations and reanalyses. *J. Climate* **16**, 4134–4143.
15. Fyfe, J. C. & Saenko, O. A., 2006 Simulated changes in the extratropical Southern Hemisphere winds and currents. *Geophys. Res. Lett.* **33**. L06701, doi:10.1029/2005GL025332.
16. Cai, W., 2006 Antarctic ozone depletion causes an intensification of the Southern Ocean super-gyre circulation. *Geophys. Res. Lett* **33**. L03712, doi:10.1029/2005GL024911.
17. Cai, W. & Cowan, T., 2007 Trends in Southern Hemisphere circulation in IPCC AR4 models over 1950–99: Ozone depletion versus greenhouse forcing. *J. Climate* **20**, 681–693.
18. Polvani, L. M., Waugh, D. W., Correa, G. J. P. & Son, S.-W., 2011 Stratospheric ozone depletion: The main drive of Twentieth-Century atmospheric circulation changes in the Southern Hemisphere. *J. Climate* **24**, 795–812.
19. Hobbs, W. R. & Raphael, M. N., 2010 Characterizing the zonally asymmetric component of the SH circulation. *Clim. Dyn.* **35**, 859–873.
20. Renwick, J. A., 2002 Southern Hemisphere circulation and relations with sea ice and sea surface temperature. *J. Climate* **15**, 3058–3068.
21. Sallée, J.-B., Speer, K. & Morrow, R., 2008 Southern Ocean fronts and their variability to climate modes. *J. Climate* **21**, 3020 – 3039.
22. Ding, Q., Steig, E. J., Battisti, D. S. & Küttell, M., 2011 Winter warming in West Antarctica caused by central tropical Pacific warming. *Nature Geosci.* **4**, 398–403.
23. Stephenson, J., G. R., Gille, S. T. & Sprintall, J., 2013 Processes controlling upper-ocean heat content in Drake Passage. *J. Geophys. Res.* In press, doi:10.1002/jgrc.20315.
24. Thoma, M., Jenkins, A., Holland, D. & Jacobs, S., 2008 Modelling circumpolar deep water intrusions on the Amundsen Sea continental shelf, Antarctica. *Geophys. Res. Lett* **35**. L18602, doi:10.1029/2008GL034939.
25. Wåhlin, A. K., Yuan, X., Björk, G. & Nohr, C., 2010 Inflow of warm Circumpolar Deep Water in the Central Amundsen Shelf. *J. Phys. Oceanogr.* **40**, 1427–1434.
26. Heimbach, P. & Losch, M., 2012 Adjoint sensitivities of sub-ice-shelf melt rates to ocean circulation under the Pine Island ice shelf, West Antarctica. *Ann. Glaciology* **53**, 59–69.
27. Gilroy, A., Mazloff, M. & Gille, S. T., 2013 The heat budget and circulation of the Amundsen Sea Embayment. *J. Geophys. Res.* Submitted.
28. Zilberman, N. V., Roemmich, D. H. & Gille, S. T., 2013 Meridional transport in the South Pacific: Assessing SAM related variability. *J. Geophys. Res.* Submitted.
29. Yin, J. H., 2005 A consistent poleward shift of the storm tracks in simulations of 21st century climate change. *Geophys. Res. Lett.* **32**. L18701, doi:10.1029/2005GL023684.
30. Oke, P. R. & England, M. H., 2004 Oceanic response to changes in the latitude of the Southern Hemisphere subpolar westerly winds. *J. Climate* **17**, 1040–1054.
31. Fyfe, J. C. & Saenko, O. A., 2005 Human-induced change in the Antarctic Circumpolar Current. *J. Climate* **18**, 3068–3073.

32. Cai, W., Shi, G., Cowan, T., Bi, D. & Ribbe, J., 2005 The response of the Southern Annular Mode, the East Australian Current, and the southern mid-latitude ocean circulation to global warming. *Geophys. Res. Lett.* **32**. L23706, doi:10.1029/2005GL024701.
33. Swart, N. C. & Fyfe, J. C., 2012 Observed and simulated changes in the Southern Hemisphere surface westerly wind-stress. *Geophys. Res. Lett.* **39**. L16711, doi:10.1029/2012GL052810.
34. Orsi, A. H., Whitworth III, T. & Nowlin Jr., W. D., 1995 On the meridional extent and fronts of the Antarctic Circumpolar Current. *Deep Sea Res., Part I* **42**, 641–673.
35. O'Neill, L. W., Chelton, D. B., Esbensen, S. K. & Wentz, F. J., 2005 High-resolution satellite measurements of the atmospheric boundary layer response to SST variations along the Agulhas Return Current. *J. Climate* **18**, 2706–2723.
36. Jiang, C., Gille, S. T., Sprintall, J., Yoshimura, K. & Kanamitsu, M., 2012 Spatial variation in turbulent heat fluxes in Drake Passage. *J. Climate* **25**, 1470–1488.
37. Chelton, D. B., DeSzoeke, R. A., Schlax, M. G., El Naggar, K. & Siwertz, N., 1998 Geographical variability of the first baroclinic Rossby radius of deformation. *J. Phys. Oceanogr.* **28**, 433–460.
38. Kohfeld, K. E., Graham, R. M., de Boer, A. M., Sime, L. C., Wolff, E. W., Quéré, L. & Bopp, L., 2013 Southern Hemisphere westerly wind changes during the Last Glacial Maximum: paleo-data synthesis. *Quar. Sci. Rev.* **68**, 76–95.
39. Moore, J. K., Abbott, M. R. & Richman, J. R., 1997 Variability in the location of the Antarctic Polar Front (90-20W) from satellite sea surface temperature data. *J. Geophys. Res.* **102**, 27825–27833.
40. Moore, J. K., Abbott, M. R. & Richman, J. R., 1999 Location and dynamics of the Antarctic Circumpolar Front from satellite sea surface temperature data. *J. Geophys. Res.* **104**, 3059–3073.
41. Kelly, K. A. & Gille, S. T., 1990 Gulf Stream surface transport and statistics at 69°W from the Geosat altimeter. *J. Geophys. Res.* **95**, 3149–3161.
42. Qiu, B., Kelly, K. A. & Joyce, T. M., 1991 Mean flow and variability of the Kuroshio Extension from Geosat altimetry data. *J. Geophys. Res.* **96**, 18,491–18,507.
43. Thompson, K. R. & Demirov, E., 2006 Skewness of sea level variability of the world's oceans. *J. Geophys. Res.* **111**.
44. Rio, M.-H. & Hernandez, F., 2004 A mean dynamic topography computed over the world ocean from altimetey, in situ measurements, and a geoid model. *J. Geophys. Res.* **109**, doi:10.1029/2003JC002226.
45. Rio, M.-H., Schaeffer, P., Moreaux, G., Lemoine, J.-M. & Bronner, E., 2009 A new Mean Dynamic Topography computed over the global ocean from GRACE data, altimetry and in-situ measurements. *OceanObs09 symposium* 21-15 September, Venice, Poster communication.
46. Pavlis, N. K., Holmes, S. A., Kenyon, S. & Factor, J. K., 2012 The development and evaluation of the Earth Gravitational Model 2008 (EGM2008). *J. Geophys. Res.* **117**. Doi:10.1029/2011JB008916.
47. Maximenko, N. A. & Niiler, P. P., 2005 Hybrid decade-mean global seal level with mesoscale resolution. In *Recent Advances in Marine Science and Technology.* (ed. N. Saxena), pp. 55 – 59. Honolulu: PACON Iinternational.
48. Griesel, A., Mazloff, M. R. & Gille, S. T., 2012 Mean dynamic topography in the Southern Ocean: Evaluating Antarctic Circumpolar Current transport. *J. Geophys. Res.* **117**. C01020 doi:10.1029/2011JC007575.
49. Hughes, C. W. & Ash, E. R., 2001 Eddy forcing of the mean flow in the Southern Ocean. *J. Geophys. Res.* **106**, 2713–2722.
50. Sokolov, S. & Rintoul, S. R., 2007 Multiple jets of the Antarctic Circumpolar Current south of Australia. *J. Phys. Oceanogr.* **37**, 1394–1412.
51. Sokolov, S. & Rintoul, S. R., 2009 Circumpolar structure and distribution of the Antarctic Circumpolar Current fronts: 1. Mean circumpolar paths. *J. Geophys. Res.* **114**. C11018, doi:10.1029/2008JC005108.
52. Sokolov, S. & Rintoul, S. R., 2009 Circumpolar structure and distribution of the Antarctic Circumpolar Current fronts: 2. Variability and relationship to sea surface height. *J. Geophys. Res.* **114**. C11019, doi:10.1029/2008JC005108.
53. Graham, R. M., de Boer, A. M., Heywood, K. J., Chapman, M. R. & Stevens, D. P., 2012 Southern ocean fronts: Controlled by wind or topography? *J. Geophys. Res: Oceans* **117**. C08018, doi:10.1029/2012JC007887.
54. Le Traon, P.-Y. & Dibarboure, G., 2004 An illustration of the contribution of the TOPEX/Poseidon–Jason-1 tandemi mission to mesoscale variability studies. *Mar. Geodesy* **27**, 3–13.

55. Dibarboure, G., Pujol, M.-I., Briol, F., Le Traon, P.-Y., Larnicol, G., Picot, N., Mertz, F. & Ablain, M., 2011 Jason-2 in DUACS: Updated system description, first tandem results and impact on processing and products. *Mar. Geodesy* **34**, 214–241.
56. Chelton, D. B. & Schlax, M. G., 2003 The accuracies of smoothed sea surface height fields constructed from tandem satellite altimeter datasets. *J. Atmos. Ocean. Tech.* **20**, 1276–1302.
57. Reynolds, R. W., Rayner, N. A., Smith, T. M., Stokes, D. C. & Wang, W., 2002 An improved in situ and satellite SST analysis for climate. *J. Climate* **15**, 1609–1625.
58. Kalnay, E., Kanamitsu, M., Kistler, R., Collins, W., Deaven, D., Gandin, L., Iredell, M., Saha, S., White, G., Woollen, J. *et al.*, 1996 The NCEP/NCAR 40-year reanalysis project. *Bull. Amer. Meteor. Soc.* **77**, 437–471.
59. Stammer, D., Cazenave, A., Ponte, R. M. & Tamisiea, M. E., 2013 Causes for contemporary regional sea level changes. *Ann. Rev. Mar. Sci.* **5**, 21–46.